

Preferential Nucleation and Self-Limiting Growth of Cu Nanoclusters on S(4 × 4)/W(111)

Qifei Wu,[†] Wenhua Chen,[‡] and Theodore E. Madey^{*,†,‡}*Department of Chemistry, Department of Physics and Astronomy, and Laboratory for Surface Modification, Rutgers, The State University of New Jersey, Piscataway, New Jersey 08854**Received: November 12, 2001; In Final Form: February 1, 2002*

The interaction of Cu with the highly ordered S(4 × 4)/W(111) surface has been studied by means of Auger electron spectroscopy (AES), low-energy electron diffraction (LEED), and scanning tunneling microscopy (STM) at room temperature. The substrate is a sulfur-induced nanoscale reconstruction of W(111) with (4 × 4) periodicity characterized by broad, planar terraces (~30 nm in width). We find that fractional monolayers of vapor-deposited Cu grow homogeneously as clusters on the S(4 × 4)/W(111) surface over a wide coverage range. At low Cu coverages (<0.1 ML), Cu nanoclusters are observed to nucleate preferentially at characteristic 3-fold hollow sites on the S(4 × 4)/W(111) surface; there is a clear energetic preference for one type of site over others. The formed Cu nanoclusters are uniform in size (~0.6 nm) as coverage increases, indicating self-limiting growth. Evidence for long-range interactions that may affect the nucleation of nanoclusters is discussed. For coverages ≥0.1 ML, additional sites are populated, and the whole surface is decorated by Cu clusters. STM data are supported by LEED and AES measurements. The results are interpreted in terms of heat of formation, relative reactivity, surface corrugation, surface diffusion, lattice mismatch, and long-range interactions in the nanoscale regime.

I. Introduction

Patterning of materials on surfaces is important in device technology and electronic fabrication. In recent years, there have been several interesting microscopic measurements and theoretical studies on the self-organization of metal and semiconductor islands on surfaces.^{1–6} The self-ordered arrays of atoms often appear in networks, and the driving forces underlying control of nanostructure organization are not fully understood. Nanostructures and quantum dots have very different properties from those of the corresponding bulk materials and can have important new applications such as changing a traditionally inert metal into a catalytically active one.⁷ Work in our laboratory has identified conditions for forming a highly ordered sulfur-induced (4 × 4) superstructure on the W(111) surface.^{8–10} The (4 × 4) superlattice is characterized by periodic arrays of sulfur clusters that are composed of approximately six sulfur atoms with a nanoscale unit distance of 1.8 nm.

Metal nucleation and growth studies on modified surfaces, especially oxide surfaces, are topics of great current interest.^{11–20} Usually, the growth modes of materials on surfaces are categorized as one of three types: layer by layer or Frank–Van der Merwe (FM), islands only or Volmer–Weber (VW), and layer plus islands or Stranski–Krastanov (SK). In particular, the growth of several transition metals (Au, Fe, Cu, etc.) on TiO₂-(110) surfaces has been extensively studied by means of X-ray photoelectron spectroscopy (XPS), low-energy ion scattering (LEIS), and high-resolution scanning electron microscopy (HRSEM) in this group during the past decade.^{17–20} For instance, Cu, Pt, Pd, and Au tend to form distinct 3D clusters on the oxide surface, exhibiting nonwetting (VW), whereas they generally wet a bare metal surface at the same temperature (FM

or SK). Furthermore, Chen et al., Xu et al., and Hansen et al. have found by scanning tunneling microscopy (STM) that 3D metal clusters often preferentially nucleate at step edges and domain boundaries of oxide surfaces.^{12–15} By comparison, much less work has been carried out on S-modified metal surfaces that are important in catalytic chemistry, petroleum chemistry, and semiconductors.^{21–25} However, it is generally believed that sulfur on the sulfide-coated surfaces changes the electronic properties of the substrate in such a way that the interaction between the adsorbate and the substrate is weakened.²¹ In a recent review article, Rodríguez and Hrbek summarized how a small concentration of sulfur atoms on a metal surface can alter the electronic properties of the surface, and then they showed that this effect has long-range character.²⁶ Pohl et al. dosed small coverages of S (<0.1 ML) on a Ag/Ru(0001) surface and found that the S atoms dislocate Ag atoms in the silver thin film on the surface and then self-organize to form a nanostructure network.³

The interaction between sulfur and catalytic metals is crucially important in oil refining. It is well-known that sulfur impurities contained in petroleum crude can poison expensive Pt-group bimetallic catalysts at great cost.²⁷ In addition, the sulfur impurities contained in widely used fuels are combusted to produce SO₂ and SO₃ that contaminate the atmosphere. In the last century, hydrodesulfurization (HDS) has been used to remove sulfur impurities from crude oil through heterogeneous catalysis and organometallic chemistry.^{28–30} Microscopically, it has been found that the HDS active sites on the widely used heterogeneous MoS₂-based catalysts can be characterized as metal–Mo–S ministructures.³¹ The catalytic activity of MoS₂ is greatly enhanced by promoters such as Ni and Co.³² It is increasingly important to understand the mechanism underlying the interaction between sulfur and metallic bonding. The knowledge obtained would be beneficial in catalyst design for

* Corresponding author. E-mail: madey@physics.rutgers.edu.

[†] Department of Chemistry and Laboratory for Surface Modification.

[‡] Department of Physics and Astronomy and Laboratory for Surface Modification.

both oil refineries and HDS reactions and thus have potential economic value.

The atomic details of the initial stages of metal growth on S-modified surfaces are particularly interesting.³³ The adsorption sites on the modified surface can be classified into different groups depending on the structure, adsorption energy, electronic properties, or reactivity on the subnanometer scale. Thanks to the development of scanning tunneling microscopy (STM) and other scanning probe microscopy (SPM) techniques during the last 20 years, nanoscale structures on surfaces can be routinely probed and imaged. In particular, it should be possible to identify the preferred adsorption sites on the surface in the initial stage of metal nucleation (submonolayer). Experimentally, the dilemma is to assign and distinguish the adsorption species from the substrate in an STM image. Namely, the new bright spots appearing in the STM image could be attributed to the adsorbate atoms or clusters, the reconstruction of the original substrate leading to displaced substrate atoms, or just occasional gas impurities. For example, there is controversy concerning the assignment of bright spots in the STM images of the MoS₂ surface because they could be assigned as either the protruding S surface atoms or the in-plane Mo.^{34,35}

In this work, we study the deposition and growth of Cu on the S(4 × 4)/W(111) superlattice surface. A model for the S(4 × 4)/W(111) surface that is based on the structure of crystalline WS₂ has been proposed;⁸ WS₂ is a component of some industrial catalysts used for HDS.²⁸ Both W and Mo are bcc metals and have many chemical similarities, including large values of heats of formation for MoS₂ and WS₂.³⁶ In this study, different scale STM images (7000, 3500, 1200, 240, and 120 Å) are obtained on Cu/S/W(111) as Cu coverage is intentionally varied from 0.05 to 2 ML. In comparison with the STM images before the metal deposition, the interaction between Cu and the S/W system has been investigated: preferential adsorption sites on the surface are identified, and evidence for the self-limiting growth of Cu nanoclusters is observed in the low-coverage range.

II. Experimental Section

The experiment is conducted in an ultrahigh vacuum (UHV) chamber equipped with instrumentation for Auger electron spectroscopy (AES) (Physical Electronics), low-energy electron diffraction (LEED) (Princeton Research), and scanning tunneling microscopy (STM) (McAllister) with a base pressure of <2 × 10⁻¹⁰ Torr. The chamber pressure is maintained by a 220-L/s ion pump (Physical Electronics), and a 110-L/s turbo molecular pump (Pfeiffer) is coupled for bakeout.

The W(111) sample is a W single-crystal disk, ~8 mm in diameter and 1 mm in thickness, that has been aligned by X-ray diffraction and then polished mechanically and chemically. The sample is supported around its edge by a semicircle of Ta wire (0.5 mm in diameter) spot-welded onto a Mo sample holder. The sample holder can be rotated 360° for processing and characterization and dropped/picked up on the STM stage via an arm on a Thermionics manipulator. The sample is cleaned by electron beam bombardment in front of the sample to >2300 K. Normally, several cycles of high-temperature flashing are required to remove C and O impurities until their AES peak ratios (relative to W) in AES spectra (3-keV electron bombardment energy) are minimal: C(272)/W(163 + 169) < 0.02 and O(503)/W(163 + 169) < 0.05. When carbon appears on the surface, O₂ gas is introduced into the UHV chamber to oxidize it during flashing. After W(111) is cleaned satisfactorily, H₂S gas (99.5%, Matheson) is introduced and adsorbed onto the W(111) surface at 5 × 10⁻⁸ Torr for 5 min (15 L) at room

temperature, following the procedure described by Nien et al.^{8,9} The covered surface is annealed to ~1100 K for 3 min by another electron beam bombardment filament located behind the sample. A pyrometer is employed to monitor the temperature of the crystal. AES and LEED measurements are performed to ensure that the S(4 × 4)/W(111) reconstruction is present. LEED patterns are recorded photographically. Usually, to get much sharper 4 × 4 LEED patterns, a second dosing of H₂S (additional 15 L) is necessary, followed by annealing and AES/LEED measurements (the modified treatment is based on refs 8 and 9). STM is used to examine the morphology of the S(4 × 4)/W(111) surface, and it is found to be routinely reproducible. The topographic mode (constant current) is adopted for collecting STM images. Images can be saved automatically. If the tunneling tip (Custom Probes Unlimited) is contaminated, it will be cleaned by field emission heating and "wild" scanning at a to-be-abandoned but fresh area of the surface (120 Å × 120 Å). Wild tunneling uses extreme conditions: high bias voltage (9500 mV), high speed, and high sensitivity in the feedback loop. In this way, contaminants can be removed from the tip.

The deposition of metal is done after a satisfactory S(4 × 4)/W(111) surface is prepared. A home-built evaporator is used to evaporate the Cu wire source (0.127 mm in diameter, 99.999%, AESAR) that is wrapped onto a 0.5-mm diameter tungsten filament. The deposition rate is estimated to be ~0.12 ML/min for Cu (see the following). The distance between the sample surface and the evaporator shutter is carefully kept constant during deposition to ensure a constant deposition rate. Different metal coverages (e.g., 0.05, 0.5, or 2 ML) are obtained by changing the deposition time on the S(4 × 4)/W(111) surface. For all experiments reported here, the S(4 × 4)/W(111) substrate is held at room temperature, ~300 K. After each deposition, AES and LEED measurements are promptly made to record the changes in chemical composition and long-range order. STM measurements are then made to observe the local structural and morphological changes. Cu coverage is calibrated approximately by using a calculation based on the relationship of the AES peak-to-peak ratio and metal coverage on the clean W(111) surface. In brief, a fractional monolayer of Cu on the clean W(111) surface has the following AES intensity relationship as a function of Cu coverage:³⁷

$$\frac{I_{\text{Cu}}}{I_{\text{W}}} = \left(\frac{I_{\text{Cu}}^0}{I_{\text{W}}^0} \right) \frac{\Theta_{\text{Cu}} \{ 1 - \exp[-a_{\text{Cu}}/\lambda_{\text{Cu}}(E_{\text{Cu}}) \cos \theta] \}}{1 - \Theta_{\text{Cu}} \{ 1 - \exp[-a_{\text{Cu}}/\lambda_{\text{Cu}}(E_{\text{W}}) \cos \theta] \}}$$

Here, I is the Auger peak magnitude; I^0 , the appropriate Auger sensitivity factor at 3 kV; Θ_{Cu} , the coverage of metal; a_{Cu} , the atomic size (2.56 Å for Cu); θ , the collection angle of the cylindrical mirror analyzer (CMA) (~46°); and $\lambda_{\text{Cu}}(E_{\text{Cu}})$ and $\lambda_{\text{Cu}}(E_{\text{W}})$, the Auger electron attenuation lengths (EAL). For Cu at 60 eV (MVV transition), $\lambda_{\text{Cu}}(E_{\text{Cu}}) \approx 2$ Å, and for W at 169 eV (NVV transition), $\lambda_{\text{Cu}}(E_{\text{W}}) \approx 3$ Å.³⁸ To obtain an accurate Auger sensitivity factor ratio between Cu and W for our experimental conditions, we have measured the intensities for the W (169 eV, NVV) peak from the clean W(111) surface and for the Cu (60 eV, MVV) peak from multilayers of Cu on the W(111) surface, giving a sensitivity ratio ($I_{\text{Cu}}^0/I_{\text{W}}^0$) ≈ 3.5 . (To illustrate the importance of using an internal standard, we note that the measured intensities of low-energy Auger electrons (e.g., Cu (60 eV, MVV)) were dramatically different on 28 different instruments, according to a report by Powell et al.³⁹). Thereafter, the coverage of submonolayer Cu on the clean W(111) surface is determined, and the deposition rate is obtained. The deposition

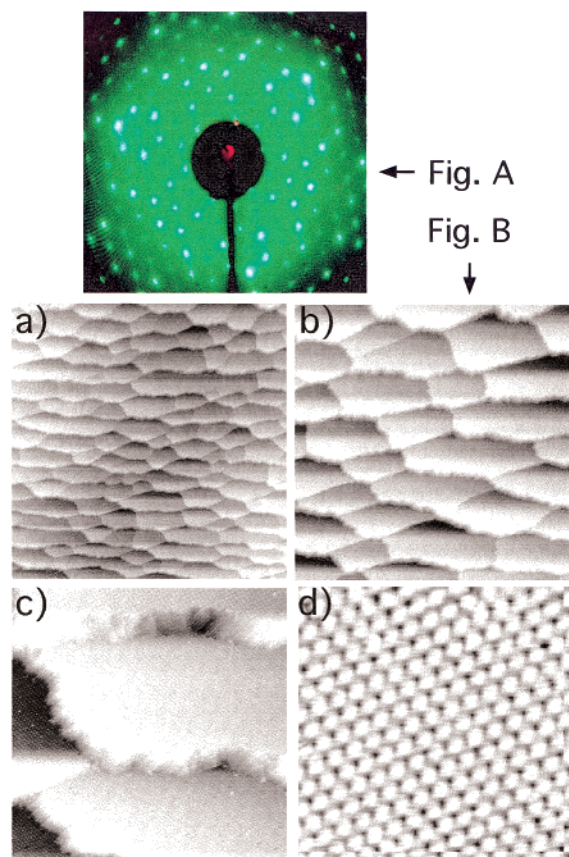


Figure 1. LEED pattern and STM images of a routinely prepared clean $S(4 \times 4)/W(111)$ surface. (a) $7000 \text{ Å} \times 7000 \text{ Å}$; (b) $3500 \text{ Å} \times 3500 \text{ Å}$; (c) $1200 \text{ Å} \times 1200 \text{ Å}$; (d) $240 \text{ Å} \times 240 \text{ Å}$. The LEED electron beam energy is 80 eV. The tunneling current is 1 or 1.2 nA, and the bias is 1000 mV.

rate on the $S(4 \times 4)/W(111)$ surface is considered to be the same as that on the clean $W(111)$ surface.

III. Results

1. Characterization of the $S(4 \times 4)/W(111)$ Surface. Figure 1 shows a LEED pattern (Fig. A) and the corresponding STM images (Fig. B) for different scanning scales of a routinely prepared $S(4 \times 4)/W(111)$ surface after two cycles of treatment on the $W(111)$ single crystal ($2 \times 15 \text{ L H}_2\text{S}$ dosing plus annealing at 1100 K; for more detailed descriptions of the clean $S(4 \times 4)/W(111)$ surface, see refs 8 and 9). Step edges and terraces are seen in the large-scale STM images ($7000 \text{ Å} \times 7000 \text{ Å}$, $3500 \text{ Å} \times 3500 \text{ Å}$, $1200 \text{ Å} \times 1200 \text{ Å}$). The $S(4 \times 4)$ terraces have an average width of $\sim 30 \text{ nm}$, and the step heights vary from single atomic height to multiautomic heights. In the $240 \text{ Å} \times 240 \text{ Å}$ image, the unit cell of the 4×4 superlattice is resolved;⁹ the lattice parameter of the (4×4) superlattice is 1.8 nm (the lattice distance of $W(111)$ is 4.47 Å). The 4×4 bright sites have been identified to be well-ordered arrays of S atoms.⁹ The structure results from the sulfur-induced reconstruction of the $W(111)$ surface. Note that the symmetry element of the surface decreases after the sulfur reconstruction although the structure is still hexagonal on the basis of LEED (i.e., from identical W atoms to distinct cluster sites and vacancy sites on the surface). An atomic-resolution STM image and the proposed model of this surface by Nien and Madey⁸⁻¹⁰ are displayed in Figure 2. They clearly show the separate adsorption areas and sites on the surface. There are up to three types of adsorption sites on this 3-fold superlattice surface, labeled as "A", "B", and "C". (Note that what we identify here as one adsorption

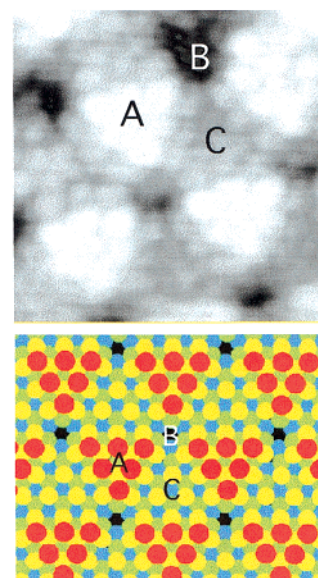


Figure 2. Atomically resolved $40 \text{ Å} \times 40 \text{ Å}$ STM image of $S(4 \times 4)/W(111)$ and the proposed model (ref 9) showing three adsorption sites (A, atop; B, vacancy; C, intermediate).

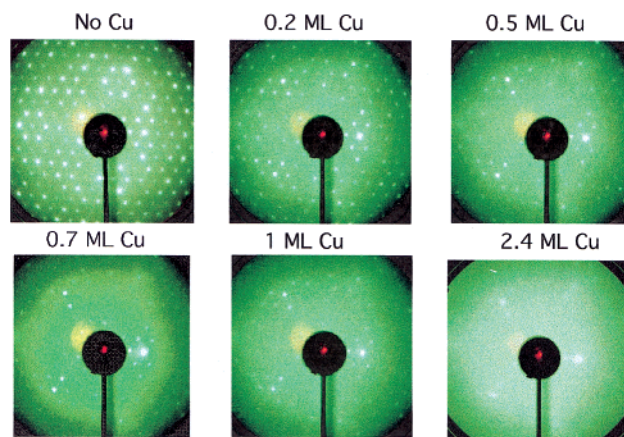


Figure 3. LEED pattern of the $S(4 \times 4)/W(111)$ surface as Cu coverage increases to 2.4 ML. The electron beam energy is 80 eV.

site corresponds to a microsurface area, not a single atop, bridging, or hollow site). A sites represent adsorption sites on top of the bright protrusions in Figure 2 that are believed to be arrays or clusters of S atoms. B sites represent vacancy adsorption sites, or dark holes, that appear to be devoid of S atoms at these locations. C sites represent intermediate adsorption sites between A and B, neither too bright nor too dark. Consistent with the evidence of Nien et al. that the outermost layer of the surface consists of S atoms,^{8,9} we have new evidence for the composition of the outermost surface layer on the basis of a low-energy ion scattering (LEIS) measurement on a similar system, $S/\text{Re}(0001)$. For H_2S doses $> 3 \text{ L}$ followed by annealing, the Re LEIS signal is reduced to less than $\sim 10\%$ of its original value; the S overlayer attenuates the substrate signal.⁴⁰ Although the LEIS experiment was performed on a different transition-metal single crystal, Re instead of W, this behavior suggests that the S overlayer covers all of the metal substrate after the saturation dosage (e.g., $30 \text{ L H}_2\text{S}$) and that there is annealing for both metal single crystals. On the other hand, the coverage of S was estimated to be $< 1 \text{ ML}$,⁸ so the sulfide-coated W layer is really an ultrathin film. Hence, the evidence indicates that atoms at the topmost layers shown in the model (Figure 2) are S, at least for the first two geometrical layers (red and yellow).

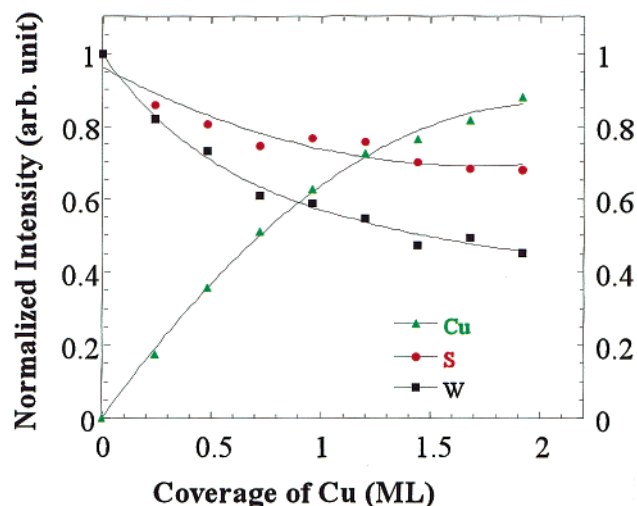


Figure 4. AES normalized intensities of Cu, S, and W as a function of Cu coverage during deposition of Cu onto $S(4 \times 4)/W(111)$ at 300 K.

2. LEED and AES Results after Dosing Cu. We have carried out systematic measurements to investigate the changes in LEED and AES signals as a function of Cu coverage for room-temperature deposition. Figure 3 demonstrates the attenu-

ation of the LEED (4×4) pattern with increasing Cu coverage up to 2.4 ML. Upon deposition of 0.2 ML Cu on the sulfide-coated $W(111)$ surface, (4×4) LEED spots are still very clear with a slight increase in the background, indicating that the $S(4 \times 4)$ structure is preserved but with some decoration. Even at 1 ML Cu, the 4×4 superlattice structure is still visible. The characteristic LEED pattern at 2.4 ML becomes a fuzzy 1×1 structure, perhaps corresponding to the diffraction spots of the partially uncovered $S(4 \times 4)$ surface where spots of the $S(4 \times 4)$ superlattice are much more attenuated than the $W(1 \times 1)$ lattice underneath.

Figure 4 shows the normalized AES intensities of Cu, S, and W signals as a function of Cu coverage. As expected, the Cu intensity increases monotonically. The intensities of S and W decrease to 70% and 45%, respectively, of their original values at 1.9 ML, so the attenuation of the W signal is faster than that of the S signal. This implies that the Cu layer selectively blocks W sites where the S overlayer is relatively thin or that some S atoms float on the Cu islands. As discussed below, STM data provide evidence for the growth of Cu as clusters on $S(4 \times 4)/W(111)$.

3. STM: High Coverage of Cu on $S(4 \times 4)/W(111)$. Figure 5 shows STM results after the deposition of 0.5 ML Cu on $S(4 \times 4)/W(111)$. In comparing the large-scale images (Figure

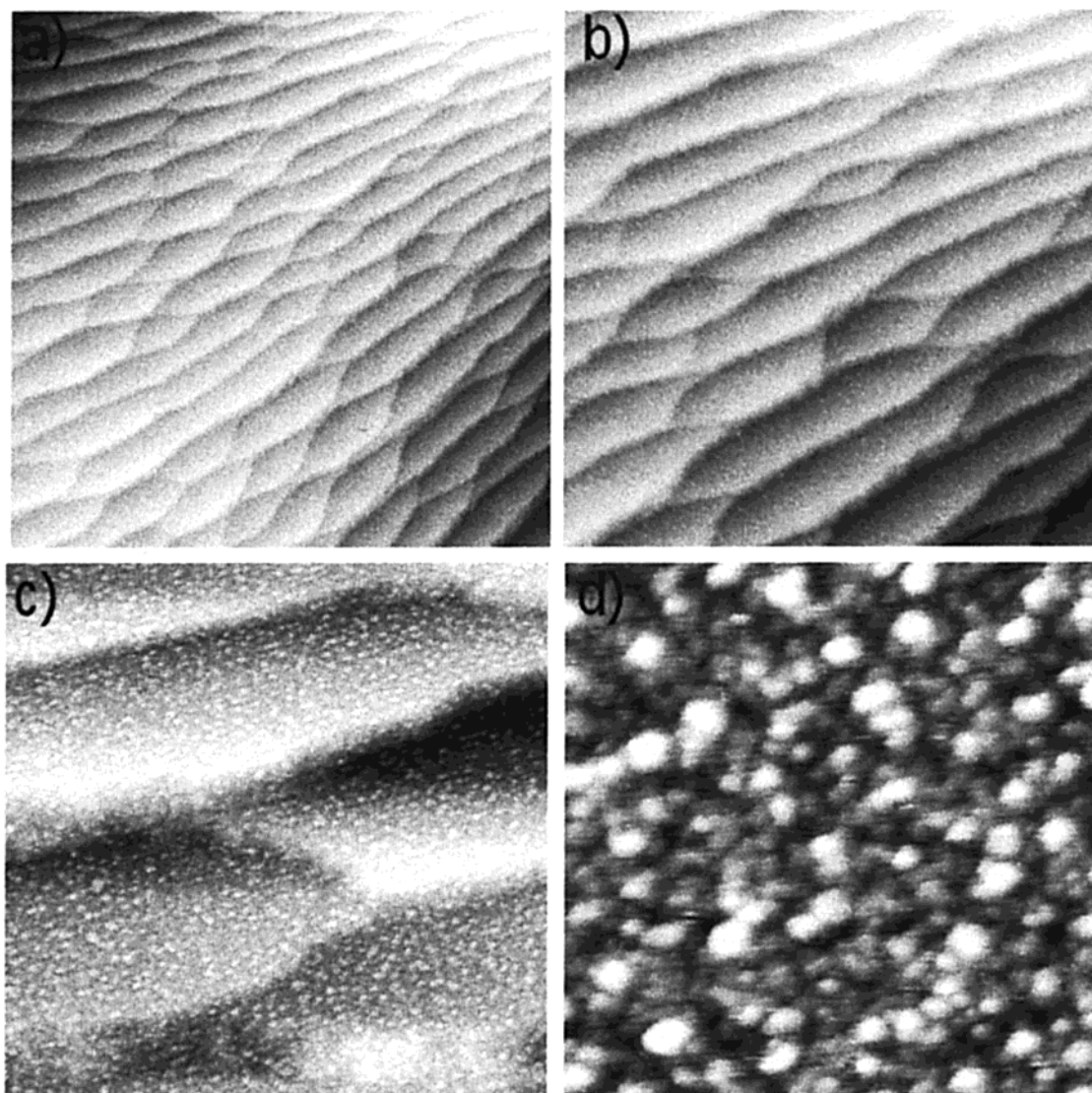


Figure 5. STM images of 0.5 ML Cu on $S(4 \times 4)/W(111)$ showing the formation of 3D Cu clusters (~ 20 Å). (a) $7000 \text{ Å} \times 7000 \text{ Å}$; (b) $3500 \text{ Å} \times 3500 \text{ Å}$; (c) $1200 \text{ Å} \times 1200 \text{ Å}$; (d) $240 \text{ Å} \times 240 \text{ Å}$.

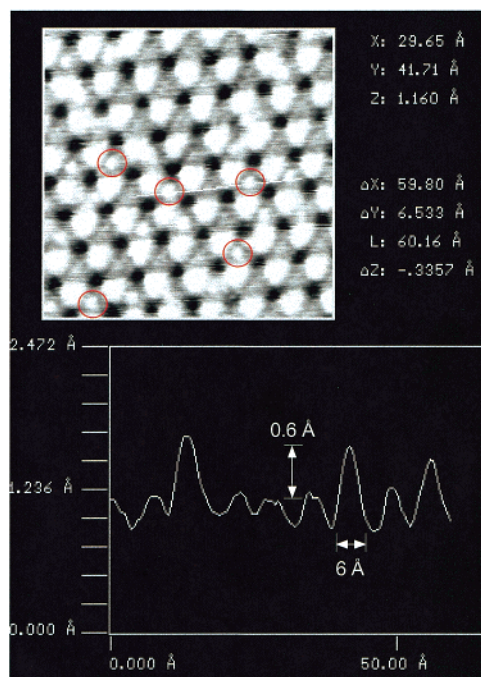


Figure 6. 120 Å \times 120 Å STM image of 0.05 ML Cu on $S(4 \times 4)/W(111)$. Nanoclusters are observed to nucleate preferentially on the intermediate sites. The size of the nanoclusters is estimated to be ~ 6 Å in diameter (x - y plane) and ~ 0.6 Å in height (z direction). A few examples are highlighted with circles in the image.

5a, 7000 Å \times 7000 Å; Figure 5b, 3500 Å \times 3500 Å) with Figure 1a and 1b, it is clear that the local overall morphology of the sulfide-coated surface, such as step edges and terraces, is not significantly changed by the deposited metal. However, there are many visible protrusions in Figure 5c (1200 Å \times 1200 Å image), which are identified as Cu clusters formed on the surface. These Cu clusters can be more clearly seen in Figure 5d (240 Å \times 240 Å image), where they are estimated to be ~ 20 Å in diameter on average. Because the diameter of a Cu atom is ~ 2.6 Å, one typical 3D cluster consists of tens or hundreds of Cu atoms. The Cu clusters seem to grow homogeneously on the terraces of the $S(4 \times 4)/W(111)$ surface, not exhibiting significant preferred adsorption near step edges. However, it is difficult to see the 4×4 superlattice structure beneath the abundant Cu cluster layer at this coverage because most of the clusters are big and bright in the STM images (the tip convolution effects magnify their real size). Therefore, we carried out low-coverage STM measurements to see the Cu clusters and the S atomic arrays at the same time.

4. STM: Low Coverage of Cu on $S(4 \times 4)/W(111)$. Figure 6 shows a 120 Å \times 120 Å high-resolution STM image after the deposition of 0.05 ML Cu on $S(4 \times 4)/W(111)$ at room temperature together with a cross-sectional analysis along a row of newly appearing nanoclusters. Here, the $S(4 \times 4)$ superlattice structure is clearly revealed and is comparable to Figure 1d. Although these STM images are not atomically resolved, as are the images in ref 9, they clearly demonstrate the surface structure modification on the nanometer scale. Separate nanoclusters appear to decorate the network of sulfur arrays, as highlighted by circles (actually they have subnanometer dimensions). The appearance of these nanoclusters is a consequence of the deposition of Cu, and we identify them tentatively as trapped Cu nanoclusters formed by the diffusion of Cu atoms along the surface. We assume for the moment that the nanoclusters consist solely of Cu atoms, although other options are explored in Discussion. These Cu nanoclusters are found to nucleate

preferentially on intermediate adsorption sites or on C initially rather than atop adsorption sites (A) and vacancy adsorption sites (B). They are extremely uniform in size. Recognizing the intrinsic error in determining cluster sizes using STM because of tip convolution, we estimate that the diameter of each uniform nanocluster is ~ 6 Å and that the apparent height is ~ 0.6 Å on the basis of the cross-sectional analysis. These results suggest that every nanocluster is a 2D array of approximately three Cu atoms (diameter of a Cu atom is ~ 2.6 Å). If we count only the Cu atoms in nanoclusters on C sites, we can estimate the coverage of Cu corresponding to images such as Figure 6 to be ~ 0.025 ML (supposing that one nanocluster contains three Cu atoms and counting, on average, ~ 20 nanoclusters in an image with dimensions of 120 Å \times 120 Å). This value is consistent with the estimated 0.05 ML that is based on AES measurements. The difference is attributed to experimental uncertainty and to the parallel population of some A sites, as discussed in the paragraph below. Note also that the Cu atomic diameter is ~ 2.6 Å and that an intermediate site measures ~ 1 nm across the center, so there is sufficient space for one intermediate site to contain three Cu atoms.

Figure 7 contains 240 Å \times 240 Å STM images of various low Cu coverages (0.05, 0.07, 0.1, and 0.2 ML) deposited on $S(4 \times 4)/W(111)$. At all of these coverages, large-area STM images such as 7000 Å \times 7000 Å and 3500 Å \times 3500 Å (not shown) appear to have the same morphology as those in Figures 1 and 5. As seen here, the 4×4 superlattice is well-resolved, and Cu clusters decorate the 4×4 superlattice clearly. The uniformity of nanoclusters on intermediate sites with increasing coverage is evidence for self-limiting growth.^{12,13} Remarkably, the nanoclusters appear to occupy rows of intermediate C sites, although isolated nanoclusters are also seen occasionally. As discussed in section IV.6, there may be a correlation between nucleation sites for nanoclusters, namely, long-range oscillatory interactions (weak force between adatoms at distances > 1 nm) that have been observed in the nanoscale range.⁴¹⁻⁴³ Moreover, at higher coverages (0.1 and 0.2 ML), extensive decoration and adsorption of Cu occurs on the other adsorption sites, such as atop sites (A) that are seen to be very bright compared to their neighbors in the same category. The adsorbed clusters at A sites can grow in size when Cu coverage increases. At 0.2 ML Cu, even several vacancy adsorption sites (B) are populated by the bright metal clusters.

We have also done complementary experiments to investigate the thermal stability of Cu nanoclusters (i.e., slight heating of $S(4 \times 4)/W(111)$ with low Cu coverages). Figure 8 shows two STM images ((a) 120 Å \times 120 Å; (b) 240 Å \times 240 Å) after the surface with 0.05 ML Cu on $S(4 \times 4)/W(111)$ is heated to ~ 600 K. After the sample is cooled to room temperature, nanoclusters with the same size and shape as those seen in Figure 6 are still present at intermediate sites, with sharp contrast from site to site. The diffusion of Cu between intermediate sites may occur during heating, but the nanoclusters seem to be stabilized on these intermediate sites after cooling. Between room temperature and ~ 600 K, adsorption on intermediate sites prevails over that on the other two sites, as revealed by the observation that the overall surface morphology shows only a minor change. However, a sharp contrast is noticeable on atop sites because some are brighter than others (Figure 8). Actually, this interesting phenomenon is weakly observable even for room-temperature STM (Figures 6 and 7a) if we carefully adjust the manual palette. It appears that atop A sites may be perturbed by adsorption of Cu atoms in the very early stages of the metal deposition, but clusters do not form until more Cu is adsorbed;

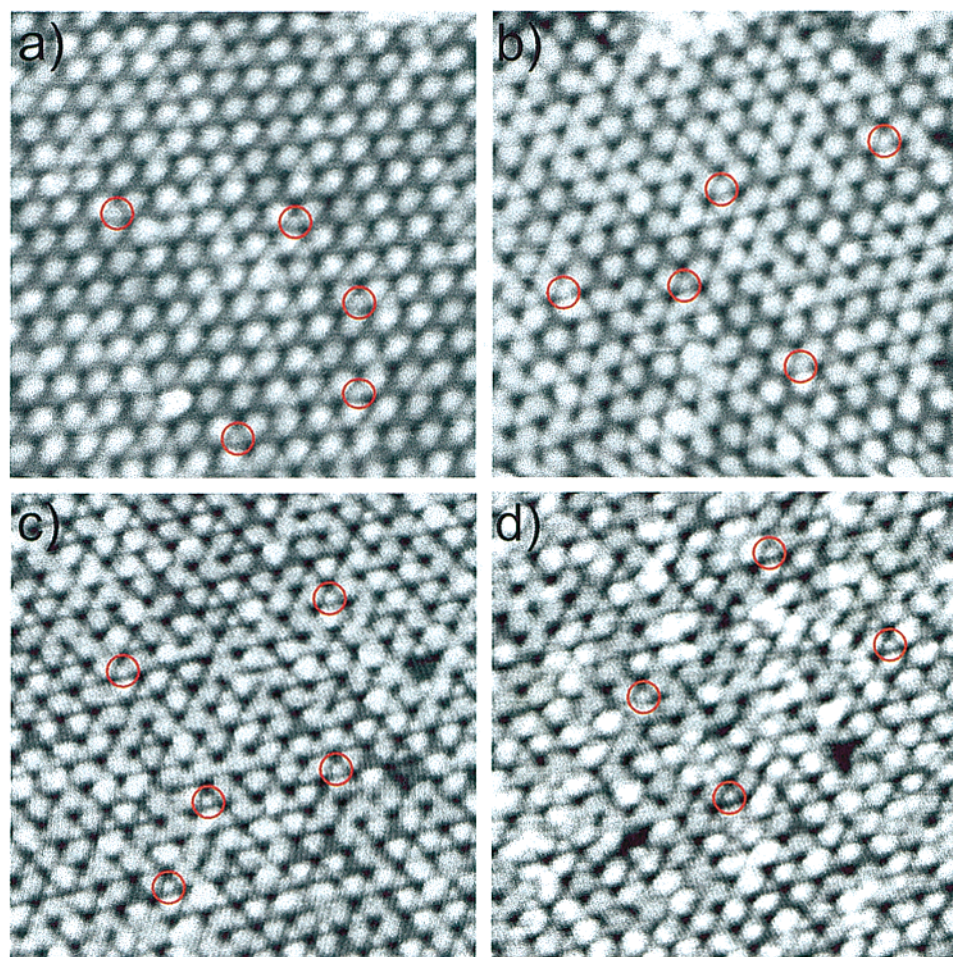


Figure 7. $240 \text{ \AA} \times 240 \text{ \AA}$ STM images of low Cu coverages on $S(4 \times 4)/W(111)$. (a) 0.05 ML; (b) 0.07 ML; (c) 0.1 ML; (d) 0.2 ML. Note that Cu nanoclusters preferentially decorate intermediate sites of the superlattice surface and remain the same size with increasing coverage as other sites are populated.

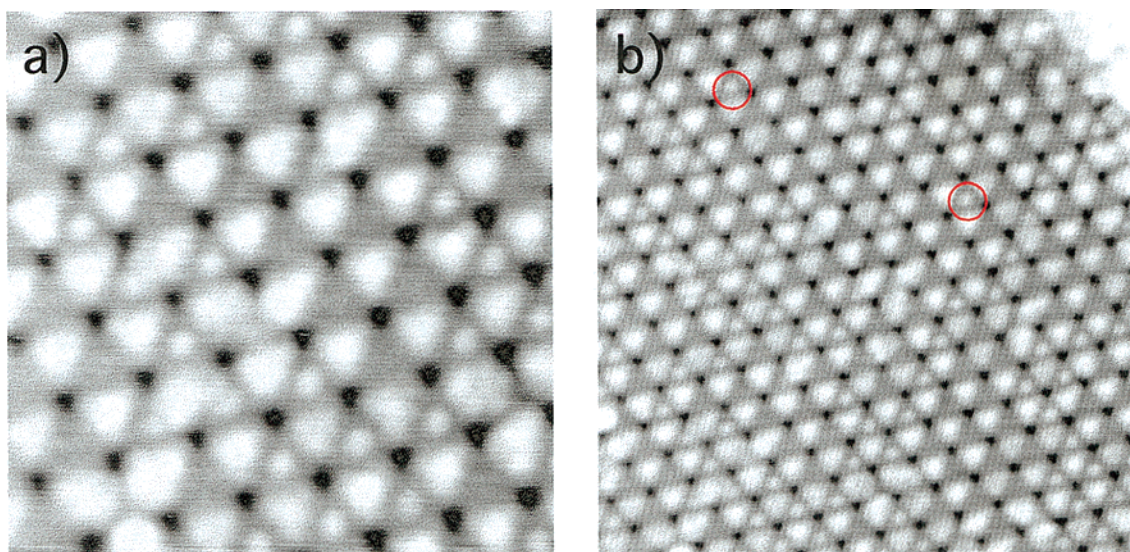


Figure 8. STM images at 0.05 ML Cu on $S(4 \times 4)/W(111)$ after heating to $\sim 600 \text{ K}$. (a) $120 \text{ \AA} \times 120 \text{ \AA}$; (b) $240 \text{ \AA} \times 240 \text{ \AA}$. Nanoclusters on intermediate sites remain on the surface. Some atop sites show obvious contrast differences. Two “isolated” nanoclusters (without nearest-neighbor nanoclusters) are highlighted with circles.

then, adsorption on atop sites (A) leads to the growth of large metal clusters (Figure 7c and d).

On the basis of STM images at 0.05, 0.07, 0.1, and 0.2 ML (Figures 7 and 8), occupancy fractions of Cu clusters can be measured on the three adsorption sites separately as a function of Cu coverage, as shown in Figure 9. Here, the number of

decorated clusters at different adsorption sites is counted, but the size of the clusters can vary dramatically from site to site at different coverages. In this histogram, the density of nanoclusters on intermediate sites seems to approach a saturation limit at 0.07 ML, which is $\sim 50\%$. It is possible that a thermodynamic steady state on intermediate sites is first achieved near 0.07 ML,

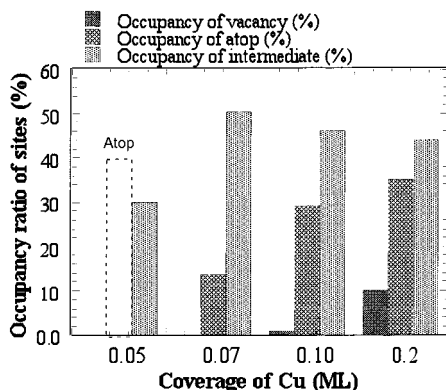


Figure 9. Occupancy fractions of three adsorption sites on $S(4 \times 4)/W(111)$ as a function of Cu coverage. The dashed bar represents the modification fraction of atop sites at 0.05 ML Cu deposition.

at which the clusters on different adsorption sites are comparable in size. In section IV.3, the STM data at 0.07 ML is used to estimate differences in adsorption energy on various sites. The A site modification at very low coverage (0.05 ML), as seen in Figures 6 and 8, is indicated in Figure 9 as a dashed bar.

IV. Discussion

We have presented STM, LEED, and AES data for the nucleation and growth of Cu on the well-ordered $S(4 \times 4)/W(111)$ surface. All of the data are consistent with one another in demonstrating cluster formation when Cu is deposited on the surface. At low coverages (≤ 0.1 ML), STM images show that Cu atoms preferentially form clusters at one characteristic site on the 3-fold sulfide-coated W surface. As Cu coverage increases, the density and the size of Cu clusters increase. At a higher coverage (0.5 ML), larger Cu clusters (e.g., 20 Å) are observed, and the cluster-formation process is supported by the LEED and AES measurements. The initial stages of Cu cluster formation are very interesting: (1) Cu forms nanoclusters preferentially on intermediate adsorption sites; (2) Cu nanoclusters show self-limiting growth; and (3) Cu clusters adsorbed on atop sites can grow in size as coverage increases.

1. Thermochemistry of Cu/S/W. Cu is reactive toward pure sulfur, and the reactivity of Cu on Ru(0001) to S (dosed as S_2) is also high on the basis of XPS and STM measurements.^{44,45} However, there is evidence that Cu is much less reactive toward sulfide-coated W or Mo surfaces. The thermochemistry of the Cu/S/W system is summarized as follows. H_2S is adsorbed on W(111) and is believed to dissociate at room temperature.⁹ H_2 desorbs completely from W(111) below 600 K,⁴⁶ leaving an S-covered surface. As a result of annealing the S-covered W(111) to 1100 K, the surface reconstructs to form the (4×4) superstructure, and the coverage is estimated to be 0.6 ML.^{8,9} Annealing at 1100 K promotes the ordering of the S overlayer and activates the bonding between S and W, probably forming WS_2 at the interface.⁸ The $S(4 \times 4)/W(111)$ surface is believed to be S-terminated according to LEIS and our previous studies.⁹ Cu is deposited onto the $S(4 \times 4)/W(111)$ surface at room temperature (~ 300 K). In considering a possible reaction between Cu adatoms and the sulfide-coated W substrate, we list the heats of formation of several sulfides in Table 1.³⁶

Apparently, a replacement reaction between the WS_2 bulk and Cu is not thermodynamically favorable. At the surface, the bond between tungsten and sulfur in WS_2 is believed to be saturated,^{28,31} so Cu might not be expected to react with WS_2 surfaces spontaneously at room temperature (~ 300 K), although surface S could be more reactive than bulk sulfide.²⁵ Low Cu/

TABLE 1: Heats of Formation of Several Metal Sulfides

metal sulfides	heat of formation (298 K) per mole of S (kJ/mol)
WS_2	-104.5
CuS	-53.1
Cu_2S	-79.4

$S/W(111)$ reactivity is supported by the study of Jaegermann et al. on the interaction of group IB metals with semiconducting metal dichalcogenide surfaces (e.g., SnS_2 , $SnSe_2$, ZrS_2 , MoS_2 , and WS_2) by XPS and LEED.⁴⁷ They concluded that there is no reaction of the deposited metal atoms with the WS_2 substrate for Cu, Ag, Au deposited at room temperature and that a metallic overlayer with an atomically abrupt semiconductor/metal interface is formed. In addition, Li. et al. observed by means of X-ray photoelectron spectroscopy that Ag deposited on molybdenum sulfide ($\sim 3-4$ ML) remains in a metallic state at < 300 K, whereas Ag can react with S multilayers (~ 8 ML) supported on Mo(110) even at 100 K.⁴⁸ Hence, it is possible that nanoclusters formed on intermediate sites of $S(4 \times 4)/W(111)$ (sulfide-coated tungsten) in the initial stages of Cu growth at room temperature are due to the nucleation of metallic Cu (by comparing the STM images in Figure 7 with those in Figure 1). The low reactivity of the nanoclusters and their thermodynamic stability are further supported by the thermal stability experiment at ~ 600 K (Figure 8).

However, we cannot rule out the possibility that Cu adsorbs initially on the S overlayer without reaction but that a small fraction of the Cu adlayer displaces S and diffuses below the surface to bind with W (e.g., forming a metal/metal interface).⁴⁷ Ohuchi et al. argued that reactive K can change the WS_2 conduction band via intercalation into WS_2 , accompanied by electron transfer.⁴⁹ Dunphy et al. found that Au can bind directly to a metal substrate by displacing S on the partially sulfide-coated Mo(100) surface.²³ Upon annealing above 400 K, Li et al. found that Ag reacts with a molybdenum sulfide surface.⁴⁸ They report that Ag overlayer atoms (~ 0.6 ML) have a tendency to penetrate into molybdenum sulfide films at temperatures > 400 K. Clark et al. believe that a significant S-Co interaction arising from charge transfer occurs for Co deposited onto S-precovered Mo(110).²² Although we do not expect extensive reaction between Cu and the S overlayer on W(111) at 300 K (on the basis of relevant literature reports and the heat of formation values (Table 1)), a localized displacement may take place at specific sites. For example, we find evidence that some atop sites are modified in the STM images at low Cu coverages (e.g., Figures 8 and 6). In addition, the different attenuation behavior of the AES normalized intensities for S and W in Figure 4 (greater attenuation of W than of S when Cu is deposited) supports a "floating S" model.²³

2. Nanoclusters I: STM Tip Effects and Stabilization in the Nanoscale Range. McIntyre et al. reported that the scanning STM tip is able to change the corrugation appearance of the $S/Pt(111)$ surface.⁵⁰ Heinze et al. reported a bias voltage-dependent corrugation reversal in STM images, for which hollow sites may appear as atoms and vice versa.⁵¹ Kushmerick et al. and Li et al. found that the STM tip assists metal-atom diffusion on the Ni/MoS_2 and $Ag/Ag(110)$ surfaces.^{31,52} In our case, many STM experiments have been performed over a 3-year period with the same apparatus using W tips in the absence of Cu deposition, but the abundant nanoclusters on intermediate sites have never been observed on the clean $S(4 \times 4)/W(111)$ surfaces either by us or by previous workers.^{8,9} The deposition of Cu is clearly responsible for the appearance of nanoclusters on intermediate sites. The STM images presented here (Figures

5–8) are quite reproducible, and most of them have several or tens of similar supporting images with small passive drifts. After moving the scan to a fresh surface area, a similar distribution of nanoclusters on intermediate sites is routinely observed promptly. The overall skeleton of the $S(4 \times 4)$ superlattice by STM shows no noticeable change before and after the low-coverage (≤ 0.2 ML) Cu deposition (Figures 1, 6, and 7). All of this data indicates that the substrate structure is unaffected by the deposition of Cu and that the distribution of Cu clusters is relatively unaffected by the STM probing processes. Under UHV conditions, the surface with nanoclusters is very stable: for several weeks, the surface morphology and cluster distribution do not appear to change if the tunneling remains uninterrupted. After thermal annealing and cooling (Figure 8), the presence of nanoclusters indicates their thermodynamic stability at intermediate sites. With elevated bias voltages (+100 to +1000 mV), the contour of nanoclusters is similar, whereas the apparent size shows small changes corresponding to the change in the distance between the surface and the STM tip. The apparent size of nanoclusters on intermediate sites may be distorted somewhat in the STM images because of tip convolution effects, but undoubtedly, nanoclusters are tiny, composed of just a few atoms.

Kushmerick et al. reported that Ni atoms freely diffuse across the MoS_2 surface at room temperature and 77 K but can be imaged at 4 K.³¹ In view of the Ni/ MoS_2 behavior and because of many cases showing the high mobility of metal atoms on flat fcc (111) surfaces,^{41,42,53,54} it is surprising that Cu nanoclusters can be trapped on the $S(4 \times 4)/\text{W}(111)$ surface and imaged at room temperature (even after annealing to 600 K) without any apparent surface diffusion of the imaged clusters. Single Cu atoms appear to diffuse readily on $S(4 \times 4)/\text{W}(111)$ and nucleate to form nanoclusters, but the nanoclusters are relative immobile. Note that the sulfide-coated $\text{W}(111)$ surface is fully covered by the nanoscale $S(4 \times 4)$ superlattice structure, which is very different from the structure of the smoother MoS_2 (0001) and fcc (111) surfaces. The $S(4 \times 4)/\text{W}(111)$ may be considered to be a superstructure of a dichalcogenide surface (i.e., WS_2 , with a deeper corrugation than that of MoS_2 (0001)). Notably, Vitali et al. reported the formation of metallic nanoclusters consisting of nine thallium adatoms on the $\text{Si}(111)-(7 \times 7)$ superlattice surface at room temperature.¹ Jarolimek et al. found that Ag atoms form small clusters inside faulted half-unit cells of the $\text{Si}(111)(7 \times 7)$ surface at room temperature.⁵⁵ Bode et al. imaged individual metallic Fe islands on a carbon (15×3) reconstructed $\text{W}(110)$ surface at room temperature.⁵⁶ Thornton et al. recently presented evidence that Cu clusters ~ 6 Å in diameter are formed upon deposition of Cu at low coverage (< 0.1 ML) onto a $\text{TiO}_2(110)$ surface held at room temperature; each cluster is identified as a 2D array of seven Cu atoms arranged in a centered hexagon that is possibly located between the bridging O rows.⁵⁷ In all of these reports indicating that tiny metal nanoclusters can be stabilized on surfaces at room temperature, it seems that a surface that is highly corrugated in the nanoscale range is necessary (e.g., unit cell distance for $\text{Si}(111)(7 \times 7)$, 2.3 nm; for C-induced $\text{R}(15 \times 3)$ on $\text{W}(110)$, 1.3 nm \times 0.7 nm;⁵⁸ for $S(4 \times 4)/\text{W}(111)$, 1.8 nm). The evidence indicates strongly that on highly corrugated or stepped superlattice structures the stabilization of metallic nanoclusters becomes possible at room temperature, whereas stabilization may not occur on relatively flat surfaces. Presumably, deep potential energy wells are expected on the potential energy

surfaces (PES) of those surfaces, which provide opportunities to effectively stabilize the metallic nanoclusters on the nanoscale networks.

3. $S(4 \times 4)/\text{W}(111)$: Three Adsorption Sites. Preferential nucleation of Cu nanoclusters on intermediate adsorption sites (C) indicates that the three types of sites on the $S(4 \times 4)/\text{W}(111)$ surface have different adsorption energies for the metal clusters. Geometrically, atop adsorption sites (A) are the most protruding among the three according to STM. Each sulfur array at an atop site is composed of six to seven sulfur atoms,^{9,10} and lateral vibrational amplitudes within this protruding array are expected to be larger than a similar array of six to seven S atoms constrained in-plane by neighboring atoms. Occasionally, a diffusing Cu atom can arrive at an atop A site and penetrate beneath the vibrating S layer, thus bonding directly with underlying W. Such stabilized Cu atoms may be the cause of the atop A-site features seen most clearly in Figure 8. Vacancy adsorption sites (B) appear to be depleted of S on the surface. Initially, we had anticipated that the B sites might be preferential adsorption sites, if such sites existed. On the basis of the STM results, adsorption of Cu on vacancy sites seems to be the least favored (Figures 7–9). However, it is possible that vacancy sites are also penetrated by single Cu atoms at low Cu coverages, similar to the behavior on atop sites, but there is no direct evidence of this in the STM images. In contrast, the configuration (or electronic structure) of S atoms at intermediate sites (C) is sufficiently different to allow the nucleation of Cu clusters and to show preferential adsorption. Perhaps the S atoms at intermediate sites can more easily exchange charge with Cu atoms and establish coordinative bonds. Another possibility is that the interaction between Cu and the subsurface W plays a role in stabilizing the nanoclusters at intermediate sites. In this case, the Cu atoms may displace the S and bond directly with W, whereas the S “floats” above the Cu. It is helpful to recall the Ni-promoted WS_2 HDS catalytic system, where a metal–metal bond between Ni and W has been suggested.²⁸ Overall, intermediate sites might have a unique atomic configuration that stabilizes metallic Cu atoms effectively.

The selective adsorption behavior of Cu reveals a potential energy difference on the 3-fold superlattice surface. Vitali et al. reported an energy difference between Tl adsorption on the faulted and unfaulted unit cell halves of $\text{Si}(111)(7 \times 7)$ on the basis of quasiequilibrium thermodynamic considerations.¹ At room temperature, a steady-state distribution for Cu nanoclusters on intermediate sites of $S(4 \times 4)/\text{W}(111)$ appears to be reached on the surface at about 0.07 ML (Figure 9). From the $240 \text{ Å} \times 240 \text{ Å}$ STM images, an occupancy fraction on intermediate sites and an occupancy fraction on atop sites are calculated; then, the energy differences between clusters on intermediate sites and similar clusters on atop sites can be roughly estimated to be ~ 0.04 eV, which is comparable to 0.075 eV reported for Tl clusters on $\text{Si}(111)(7 \times 7)$ by Vitali et al. (the calculation is based on the Boltzmann distribution).¹ We anticipate that the potential energy differences between intermediate sites and vacancy sites are even larger. The potential energy differences between different sites could be important during the initial stage of metal adsorption, which contributes to the self-organization of metallic nanoclusters on intermediate sites. It also reflects the importance of the local atom arrangement on surfaces, which determines different chemical behavior and electronic properties.

4. Nanoclusters II: Self-Limiting Growth and Perturbation of Atop Sites. Cu nanoclusters on intermediate sites are uniform in size with increasing coverage (Figure 7), demonstrating self-limiting growth.^{12,13} Chen et al. have recently reported

self-limiting growth behavior for the growth of Cu and Ag islands on TiO₂(110) below 0.5 ML.^{12,13} Their evidence for self-limiting growth is the observation that the size of the metal islands remains almost constant but the island density increases with increasing coverage. This observation is quite comparable to our results, except for (1) the difference in the size—Cu clusters formed on TiO₂(110) are 3D and are composed of hundreds of Cu atoms, whereas those on the sulfide-coated tungsten are 2D and are composed of several Cu atoms—and (2) the homogeneity of the clusters, which is discussed in the following text. On the basis of the STM images (Figures 6 and 8), Cu nanoclusters appear to be tiny, perhaps as small as trimers of metal. Considering that the width of one intermediate site is about 1 nm, only a fraction of the intermediate sites are occupied by Cu nanoclusters (≤ 6 Å in diameter). When more Cu atoms are dosed onto the surface, they do not bind with the existing nanoclusters on intermediate sites, which suggests that a lattice mismatch may exist between Cu islands and the substrate atoms in intermediate sites. Crystalline fcc Cu has a lattice constant a of 2.56 Å, and the surface S—S distance b is 3.187 Å on WS₂,^{28,36} so the lattice mismatch, $(b - a)/b$, is $\sim 20\%$ (if we consider that S pseudomorphically grows on W(111) with a lattice distance of 4.47 Å, the lattice mismatch is $\sim 42\%$).⁵⁹ This lattice mismatch and accompanying surface strain can be crucial in hindering further Cu nucleation and limiting the growth of tiny Cu islands. As indicated above, it is also possible that the potential energy barrier in the highly corrugated S(4 × 4) superlattice limits the further growth of nanoclusters.

However, it is useful to consider related work on interactions of metal with sulfur-modified surfaces. Hrbek et al. argued that for Au deposition on S-precovered Ru(0001) Au atoms displace S adatoms and compress S domains, suggesting a net repulsive interaction between neighboring Au and S islands mediated by the Ru substrate.²⁴ Dunphy et al. believed that competition for binding sites with the Mo substrate leads to repulsive interactions between coadsorbed S and Au atoms.²³ For S(4 × 4)/W(111), the entire surface is identified as being terminated by chemically saturated S. We suggest that lattice mismatch between a tiny Cu island and the S array at an intermediate site is an important fact that suppresses the further growth of Cu nanoclusters, leading to self-limiting growth.

Many atop sites show some modification (i.e., increased brightness in STM images) after very low Cu coverage (0.05 ML), according to the contrast difference in Figure 8 as well as that in Figure 6 if the manual palette for the image is adjusted. The contrast difference between various atop sites is negligible on the clean S(4 × 4)/W(111) surface with variable palettes (see Figure 1d and the corresponding images). The frequent appearance (see the dashed bar in Figure 9) of the modification excludes the possibility that it is due to occasional gas molecules and impurities on the surface. One possibility is that the modification may be attributed to the adsorption of one or two Cu atoms. As suggested in the previous section, perhaps Cu penetrates atop sites during the molecular vibration of the S arrays (the diameter of atop sites is 8 Å) and becomes stabilized; S atoms at atop sites can expand outward to accommodate Cu more efficiently than can those at intermediate sites, which are relatively constrained. This behavior is consistent with the suggestions of Dunphy et al. and Hrbek et al. that deposited metal can displace and compress S to a higher-coverage structure.^{23,24} Second, a less-likely possibility is that the contrast difference arises from the adsorption of Cu nanoclusters on intermediate sites; they may alternatively perturb the electronic density of neighboring atop S arrays through long-range

interactions, as detected by STM. Rodriguez et al. report that theoretical studies predict long-range character of the electronic perturbations induced by S.²⁶

5. Nanoclusters III: Critical Size Analysis. The formation of metallic Cu nanoclusters on S(4 × 4)/W(111) at coverages ≤ 0.2 ML is consistent with the reported weak interactions between certain metals and sulfide-coated metal substrates.²¹ The surface energy of Cu (γ_{Cu}) is ~ 1.7 J/m,^{2,60} and the surface energy of the sulfide-coated W(111) ($\gamma_{\text{S/W}}$) is expected to be small (on the scale of a few tenths of 1 J/m²), so Cu atoms are expected to nucleate as clusters on the surface. If we assume that the cluster-formation process can be described as homogeneous capillary nucleation, then we can calculate the critical cluster size (r^*) for the formation of stable nuclei:⁶¹

$$r^* = -\left(\frac{2\gamma}{\Delta G_v}\right) = \frac{2\left(\frac{4}{3}\pi a_{\text{Cu}}^3\right)(\gamma_{\text{Cu}} - \gamma_{\text{S/W}})}{kT_s \ln \frac{p}{p_0}}$$

Here, a_{Cu} is the radius of a Cu atom, 1.28 Å; T_s , the substrate temperature, 300 K; k , Boltzmann's constant, 1.38×10^{-23} J/K; p_0 , the vapor pressure of Cu at room temperature, 10^{-46} Torr;^{36,62} and p , the effective vapor pressure of Cu from the doser, $\sim 10^{-9}$ Torr (assuming that a deposition rate of 1 ML/s corresponds to $\sim 10^{-6}$ Torr and that our deposition rate is ~ 0.12 ML/min). At 300 K, r^* is estimated to be ~ 0.7 Å, which is less than the radius of a Cu atom. We realize that this calculation is just a rough estimation of the critical cluster size for Cu on S(4 × 4)/W(111); however, it supports the proposition that small clusters containing very few atoms may be formed and stabilized on the surface (e.g., the nanoclusters formed from a few Cu atoms on the intermediate sites of S(4 × 4)/W(111)).

6. Nanoclusters IV: Long-Range Interactions. As mentioned in section III.4, it seems from Figure 7 that nanoclusters appear in rows and groups; there are few "isolated" nanoclusters that lack nearest neighbors (note that two isolated nanoclusters are highlighted in Figure 8b). This behavior suggests that long-range interactions (>1 nm) may somehow influence the nucleation of nanoclusters as neighbors to existing nanoclusters (more discussion is at the end of this section).⁴³ The distance between nearest-neighbor nanoclusters is the (4 × 4) unit cell dimension, 1.8 nm. We use simple statistical arguments in an attempt to provide insights into the question of long-range interactions. Each nanocluster in a C site is surrounded by six nearest-neighbor C sites. An isolated nanocluster occurs when none of the six nearest-neighbor sites is occupied by other nanoclusters. The probability of finding an isolated nanocluster (P_{IN}) on a surface lattice can be expressed as

$$P_{\text{IN}} = x(1 - x)^n$$

where x is the probability that a given site is occupied, $(1 - x)$ is the probability that a nearest-neighbor site is unoccupied, and n is the number of possible nearest-neighbor sites ($n = 6$ in the present case). At 0.05 ML Cu coverage, the fraction of occupied C sites is 0.3 (Figure 9), so $x = 0.3$; $(1 - x) = 0.7$ is the probability that a C site is unoccupied. Thus,

$$P_{\text{IN}} = 0.3(0.7)^6 = 0.04$$

One would therefore expect $\sim 4\%$ of nanoclusters to be isolated if nucleation and growth are random. From five STM images (240 Å × 240 Å) for 0.05 ML Cu on S(4 × 4)/W(111), we estimate the experimental P_{IN} to be 0.02 ± 0.01 (i.e., Figure

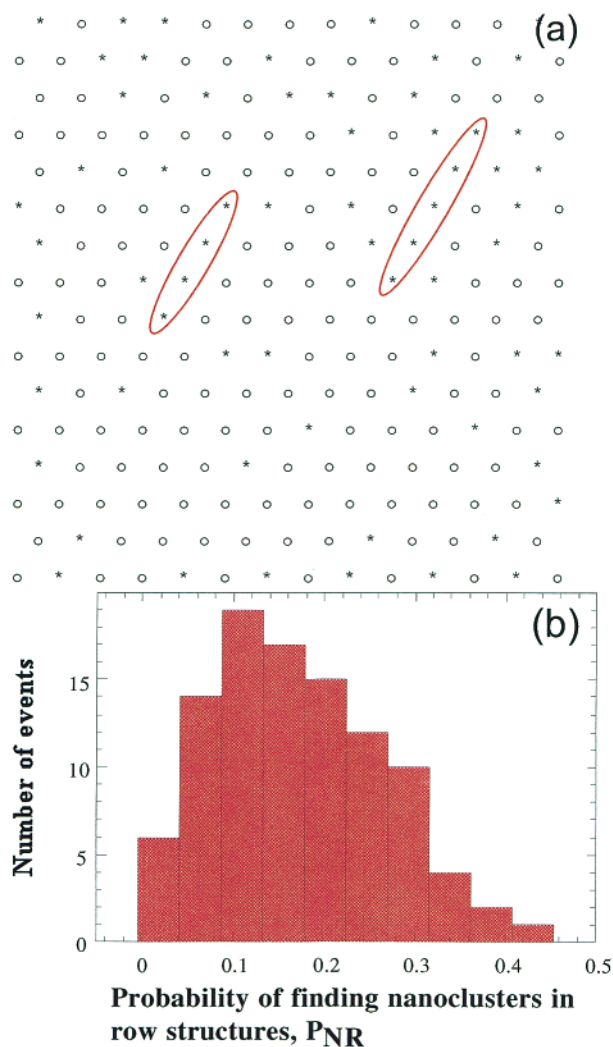


Figure 10. (a) One simulated image showing the appearance of nanoclusters using a random cluster-growth model (stars correspond to nanoclusters and ovals correspond to unoccupied intermediate sites). Note that “row structures” of nanoclusters are highlighted. (b) Histogram of the probability of finding nanoclusters in row structures (number of events vs P_{NR} (see text)). Data are based on 100 simulations, each of which is similar to that in (a).

8b and four additional images in the same experimental sequence). Although the data suggest that nucleation of nanoclusters in C sites may be a nonrandom process, the difference between the calculated and observed values of P_{IN} is too small to be statistically significant.

In a further attempt to search for statistical evidence that nanoclusters nucleate at sites adjacent to other nanoclusters, we have performed a simulation of random cluster growth on a hexagonal lattice. Our aim is to estimate the probability that clusters form 1D rows containing four or more nanoclusters. First, we construct a hexagonal lattice with 216 lattice dots in a square (see Figure 10a). Each lattice dot represents an intermediate site of $S(4 \times 4)/W(111)$ (according to the $240 \text{ \AA} \times 240 \text{ \AA}$ STM image, about 220 intermediate sites are counted on average; see Figures 7 and 8). Second, all lattice dots in the square are numbered. Third, using a random-number generator, 65 random numbers between 1 and 216 are obtained; these numbers identify the sites filled by a random-cluster nucleation process on lattice dots of the hexagonal lattice ($65/216 = 0.3$, satisfying the experimental occupancy fraction of intermediate sites at 0.05 ML; see Figure 9). Figure 10a shows a typical simulated result; stars and ovals represent occupied and unoc-

cupied intermediate sites, respectively. (To test the simulation results, we have found the expected value for P_{IN} in the simulated images to be 0.04 ± 0.02 , in good agreement with the calculated value, $P_{IN} = 0.04$). Fourth, we examine the appearance probability of nanoclusters in rows, so-called “row structures” in these simulations. A row structure is defined to consist of at least four nanoclusters in a row, as indicated in the highlighted regions in Figure 10a. Row structures are aligned nanoclusters without gaps—four in a row, five in a row, six in a row, and so on. Fifth, we calculate the probability of finding nanoclusters in row structures (P_{NR}).

The P_{NR} calculation is made as follows. For each simulation, we count the number of nanoclusters in the rows containing four or more; we avoid double counting in intersecting rows. Then, we divide the sum by 65, the total number of nanoclusters in the simulation area, which gives a value of $0 < P_{NR} < 1.00$ for one simulation. We repeat this procedure for each of 100 simulations; the results (number of events vs P_{NR}) are plotted in the histogram of Figure 10b. The most probable value of P_{NR} is ~ 0.1 ; the average value is 0.17, with a standard deviation of 0.09. The largest value of P_{NR} observed in any simulation is 0.42.

On the basis of the analysis of the experimental results (the same five STM images that were indicated above), the experimental average value of P_{NR} is 0.36 ± 0.09 . Note that the five STM images used for comparison are obtained after the room-temperature-deposited sample is thermally annealed at $\sim 600 \text{ K}$ (see text regarding Figure 8). For the best-resolved image (Figure 8b), we obtain $P_{NR} = 0.57$. Although the statistics are poor, it appears that nanoclusters in STM images are observed to be in rows with a higher frequency than expected from a random nucleation process.

Recently, the physics of long-range interactions in 2D layers has been demonstrated clearly through field ion microscopy (FIM) by Koh and Ehrlich.⁴³ They found that when single metal atoms of Ir and Pd are dosed onto a $W(110)$ surface they incorporate into chains of Ir and Pt, respectively. The adatoms move more or less parallel to the chains without coming close to the chain side but incorporate only at the end of chains, guided by long-range interactions. Basically, the long-range interaction between adatoms and small clusters can affect the potential energy surface (PES) over which adatom diffusion occurs and thus can determine the ultimate adsorption and binding site. Koh and Ehrlich conclude that “in the vicinity of growing entities, long-range interactions between adatoms and surface clusters will, in general, have a significant effect upon atomic kinetics”.⁴³ In our STM studies, we are not able to monitor real-time processes (dynamics) during adsorption, diffusion, and nucleation of Cu atoms or nanoclusters, but we can collect information about the statistical distribution of Cu nanoclusters after deposition. On the basis of a simulation of random cluster growth and its comparison with the STM data for Cu nanocluster formation, we tentatively suggest that long-range interactions may affect the deposition and nucleation processes of Cu atoms and nanoclusters on $S(4 \times 4)/W(111)$ and lead to the observed distribution of nanoclusters. The nature of the interactions is not clear and could involve such factors as long-range perturbations of surface strain or of local electron density. We realize that the STM images available for analysis are relatively limited compared to the simulations. In later experiments, we will focus on obtaining more extensive data sets (both simulations and experiments) to clarify this interesting issue.

7. Late-Stage Cluster Growth: Occupancy of Other Adsorption Sites and Homogeneity. The density of nanoclus-

ters on intermediate sites seems to approach a saturation limit, 50% at ~0.07 ML in the histogram of Figure 9. The stabilizing ability of intermediate sites seems to saturate at a critical coverage of Cu (~0.07 ML), above which the other adsorption sites increase in occupancy. The occupancy fraction of atop sites increases especially quickly at ≥0.07 ML. Several possibilities may be associated with this behavior: (a) Cu clusters nucleate at atop sites that have already been occupied by single Cu atoms at early stages of deposition; (b) Cu atoms adsorb on special atop sites that are already surrounded by several Cu nanoclusters; (c) S atoms are compressed and displaced further by Cu, leading to the floating of S atoms that are seen as protruding in STM images. Because the S(4 × 4) superlattice structure survives at ≤0.2 ML (still resolved in STM images), we believe that the extra bright features on most adsorption sites are mostly metallic Cu. The occupancy at vacancy sites becomes visible at ~0.1 ML, possibly because of the coalescence of neighboring big clusters (i.e., those on atop sites). The nucleation of Cu clusters on atop sites is not a form of self-limiting growth because these clusters can spread over and coalesce on the surface, as is obvious in Figure 7d. This growth behavior takes place mainly in the later stage of cluster formation. At 0.5 ML, clusters grow homogeneously on the surface to sizes as large as 20 Å after ripening and coalescing (Figure 5).

The observation of homogeneous growth of Cu clusters on the S(4 × 4)/W(111) surface at 0.5 ML (Figure 5) is an interesting byproduct of this study. Large clusters are distributed everywhere on terraces of the surface, irrespective of step edges or plane terraces. This result is in contrast with the heterogeneous growth of metal islands (Cu, Au, etc.) on oxide surfaces (e.g., TiO₂), where islands are often found predominantly near step edges and domain boundaries on surfaces.^{12–14} Presumably in the initial stage of growth (≤0.2 ML), Cu nanoclusters nucleate directly on the highly corrugated S(4 × 4) nanoscale network, showing no special affinity for step edges, so homogeneous 3D cluster growth is observed in the late stages of growth (0.5 ML).

8. Future Outlook and Applications. The Cu/S(4 × 4)/W(111) surface at low coverage may have interesting physical and chemical properties and may be a model nanoscale catalyst system. Because hydrodesulfurization (HDS) is usually catalyzed by metal-promoted molybdenum and tungsten sulfides,^{28,31,32,34,63} the metal-dosed S(4 × 4)/W(111) surface could show interesting catalytic activity. A study of the surface reactivity toward organic S compounds (e.g., thiophene) before and after the metal decoration would also be interesting. In addition, preferential nucleation of Cu nanoclusters on S(4 × 4)/W(111) may form an array of metallic nanodot structures. We plan to search for evidence of metallic behavior, self-limiting growth, and long-range interactions of nanoscale features for other metals deposited onto S(4 × 4)/W(111).

V. Conclusions

The physical deposition of Cu on a S(4 × 4)/W(111) superlattice surface has been studied at room temperature. In the very low Cu coverage range (<0.1 ML), Cu atoms preferentially decorate one type of site (intermediate) on the 3-fold surface; 2D nanoclusters composed of Cu are produced on the surface and are characterized to be uniform in size (~0.5 nm in diameter) on the 4 × 4 superlattice. The adsorption-site specificity is believed to be a reflection of the potential energy difference for the different adsorption sites on the nanoscale surface. The stabilization of metallic nanoclusters at room temperature is related to the fact that the S(4 × 4)/W(111)

surface is highly corrugated on the nanometer scale. The growth of Cu nanoclusters is self-limited at low Cu coverages, which may be attributed to a lattice mismatch between the metal and S on the surface or to a potential energy barrier surrounding nanoclusters on the highly corrugated superlattice surface. The observed modification of atop sites at very low coverages is thought to be due to direct single Cu atom adsorption or to the electronic density perturbations induced by metal nanoclusters at intermediate sites. As Cu coverage increases (≥0.1 ML), cluster formation occurs on the other adsorption sites (atop and vacancy). Possible long-range interactions among Cu nanoclusters are discussed in the context of a simulation of a random cluster-growth model; there is evidence for nonrandom nucleation of nanoclusters on the annealed surface at low coverage (0.05 ML). At the highest Cu coverage studied here (0.5 ML), large 3D clusters (20 Å in diameter) are found to grow homogeneously on the surface and exhibit late-stage cluster growth and coalescence.

Acknowledgment. We thank C.-H. Nien and K. Pelhos for their help during the early stages of these experiments. We are grateful to B. Yakshinskiy for measuring the LEIS data. R. Barnes is acknowledged for her enlightening suggestions about our statistical analysis of simulations. This program has been supported by the Office of Basic Energy Sciences, U.S. Department of Energy (DOE).

References and Notes

- (1) Vitali, L.; Ramsey, M. G.; Netzer, F. P. *Phys. Rev. Lett.* **1999**, *83*, 316.
- (2) Brune, H.; Giovannini, M.; Bromann, K.; Kern, K. *Nature (London)* **1998**, *394*, 451.
- (3) Pohl, K.; Bartelt, M. C.; de la Figuera, J.; Bartelt, N. C.; Hrbek, J.; Hwang, R. Q. *Nature (London)* **1999**, *397*, 238.
- (4) Springholz, G.; Holy, V.; Pinczolis, M.; Bauer, G. *Science (Washington, D.C.)* **1998**, *282*, 734.
- (5) Venezuela, P.; Tersoff, J.; Floro, J. A.; Chason, E.; Follstaedt, D. M.; Liu, F.; Lagally, M. G. *Nature (London)* **1999**, *397*, 678.
- (6) Preobrajenski, A. B.; Barucki, K.; Chassé, T. *Phys. Rev. Lett.* **2000**, *85*, 4337.
- (7) Valden, M.; Lai, X.; Goodman, D. W. *Science (Washington, D.C.)* **1998**, *281*, 1647.
- (8) Nien, C.-H.; Madey, T. E. *Surf. Sci.* **1999**, *254*, 433–435.
- (9) Nien, C.-H.; Abdelrehim, I. M.; Madey, T. E. *Surf. Rev. Lett.* **1999**, *6*, 77.
- (10) Madey, T. E.; Nien, C.-H.; Pelhos, K.; Kolodziej, J. J.; Abdelrehim, I. M.; Tao, H.-S. *Surf. Sci.* **1999**, *438*, 191.
- (11) Cosandey, F.; Madey, T. E. *Surf. Rev. Lett.* **2001**, *8*, 73.
- (12) Chen, D. A.; Bartelt, M. C.; Seutter, S. M.; McCarty, K. F. *Surf. Sci.* **2000**, *464*, L708.
- (13) Chen, D. A.; Bartelt, M. C.; Hwang, R. Q.; McCarty, K. F. *Surf. Sci.* **2000**, *450*, 78.
- (14) Xu, C.; Lai, X.; Zajac, G. W.; Goodman, D. W. *Phys. Rev. B* **1997**, *56*, 13464.
- (15) Hansen, K. H.; Worren, T.; Stempel, S.; Lægsgaard, E.; Bäumer, M.; Freund, H.-J.; Besenbacher, F.; Stensgaard, I. *Phys. Rev. Lett.* **1999**, *83*, 4120.
- (16) Charlton, G.; Howes, P. B.; Muryn, C. A.; Raza, H.; Jones, N.; Taylor, J. S. G.; Norris, C.; McGrath, R.; Norman, D.; Turner, T. S.; Thornton, G. *Phys. Rev. B* **2000**, *61*, 16117.
- (17) Pan, J. M.; Diebold, U.; Zhang, L. Z.; Madey, T. E. *Surf. Sci.* **1993**, *295*, 411.
- (18) Diebold, U.; Pan, J. M.; Madey, T. E. *Surf. Sci.* **1993**, *287*, 896.
- (19) Diebold, U.; Pan, J. M.; Madey, T. E. *Surf. Sci.* **1995**, *333*, 845.
- (20) Zhang, L.; Persaud, R.; Madey, T. E. *Phys. Rev. B* **1997**, *56*, 10549.
- (21) Wormeester, H.; Hüger, E.; Bauer, E. *Phys. Rev. Lett.* **1998**, *81*, 854.
- (22) Clark, P. G.; Friend, C. M. *J. Chem. Phys.* **1999**, *111*, 6991.
- (23) Dunphy, J. C.; Chapelier, C.; Ogletree, D. F.; Salmeron, M. B. *J. Vac. Sci. Technol., B* **1994**, *12*, 1742.
- (24) Hrbek, J.; Schmid, A. K.; Bartelt, M. C.; Hwang, R. Q. *Surf. Sci.* **1997**, *385*, L1002.
- (25) Hrbek, J.; de la Figuera, J.; Pohl, K. J. T.; Rodriguez, J. A.; Schmid, A. K. B. N. C.; Hwang, R. Q. *J. Phys. Chem. B* **1999**, *103*, 10557.
- (26) Rodriguez, J. A.; Hrbek, J. *Acc. Chem. Res.* **1999**, *32*, 719.

- (27) Somorjai, G. A. *Introduction to Surface Chemistry and Catalysis*; Wiley: New York, 1994.
- (28) Startsev, A. N. *Catal. Rev.—Sci. Eng.* **1995**, *37*, 353.
- (29) Friend, C. M.; Chen, D. A. *Polyhedron* **1997**, *16*, 3165.
- (30) Bianchini, C.; Meli, A. *Acc. Chem. Res.* **1998**, *31*, 109.
- (31) Kushmerick, J. G.; Weiss, P. S. *J. Phys. Chem. B* **1998**, *102*, 10094.
- (32) Rodriguez, J. A.; Dvorak, J.; Capitano, A. T.; Gabelnick, A. M.; Gland, J. L. *Surf. Sci.* **1999**, *429*, L462.
- (33) McCarty, G. S.; Weiss, P. S. *Chem. Rev.* **1999**, *99*, 1983.
- (34) Kushmerick, J. G.; Kandel, S. A.; Johnson, J. A.; Weiss, P. S. *J. Phys. Chem. B* **2000**, *104*, 2980.
- (35) Fuhr, J. D.; Sofo, J. O.; Saúl, A. *Phys. Rev. B* **1999**, *60*, 8343.
- (36) *CRC Handbook of Chemistry and Physics*, 72nd ed.; Lide, D. R., Ed.; CRC Press: Boca Raton, FL, 1991–1992.
- (37) Briggs, D.; Seah, M. P. *Practical Surface Analysis*; Wiley: New York, 1996.
- (38) Powell, C. J.; Jablonski, A. J. *J. Phys. Chem. Ref. Data* **1999**, *28*, 19.
- (39) Powell, C. J.; Erickson, N. E.; Madey, T. E. *J. Electron Spectrosc. Relat. Phenom.* **1982**, *25*, 87.
- (40) Yakshinskiy, B.; Madey, T. E. Unpublished results.
- (41) Kellogg, G. L. *Surf. Sci. Rep.* **1994**, *21*, 1.
- (42) *Surface Mobilities on Solid Materials*; Binh, V. T., Ed.; Plenum Press: New York, 1983; p 103.
- (43) Koh, S. J.; Ehrlich, G. *Phys. Rev. Lett.* **2001**, *87*, 106103–106106.
- (44) Kuhn, M.; Rodriguez, J. A. *J. Phys. Chem.* **1994**, *98*, 12059.
- (45) de la Figuera, J.; Pohl, K.; Schmid, A. K.; Bartelt, N. C.; Hrbek, J.; Hwang, R. Q. *Surf. Sci.* **1999**, *93*, 433–435.
- (46) Madey, T. E. *Surf. Sci.* **1972**, *29*, 571.
- (47) Jaegermann, W.; Ohuchi, F. S.; Parkinson, B. A. *Surf. Interface Anal.* **1988**, *12*, 293.
- (48) Li, S. Y.; Rodriguez, J. A.; Hrbek, J.; Huang, H. H.; Xu, G.-Q. *Surf. Sci.* **1998**, *395*, 216–228.
- (49) Ohuchi, F. S.; Jaegermann, W.; Pettenkofer, C.; Parkinson, B. A. *Langmuir* **1989**, *5*, 439.
- (50) McIntyre, B. J.; Sautet, P.; Dunphy, J. C.; Salmeron, M.; Somorjai, G. A. *J. Vac. Sci. Technol., B* **1994**, *12*, 1751.
- (51) Heinze, S.; Blugel, S.; Pascal, R.; Bode, M.; Wiesendanger, R. *Phys. Rev. B* **1998**, *58*, 16432.
- (52) Li, J.; Berndt, R.; Schneider, W.-D. *Phys. Rev. Lett.* **1996**, *76*, 1888.
- (53) Brune, H.; Bales, G. S.; Jacobsen, J.; Boragno, C.; Kern, K. *Phys. Rev. B* **1999**, *60*, 5991.
- (54) Kyuno, K.; Ehrlich, G. *Phys. Rev. Lett.* **2000**, *84*, 2658.
- (55) Jarolimek, T.; Myslivecek, J.; Sobotik, P.; Ost'adal, I. *Surf. Sci.* **2001**, *386*, 482–485.
- (56) Bode, M.; Pascal, R.; Wiesendanger, R. *Z. Phys. B: Condens. Matter* **1996**, *99*, 143.
- (57) Thornton, G.; Brookes, I.; Raza, H.; Pang, C. L.; Haycock, S. *Kinetics and Dynamics of Substrate and Metal Atoms on TiO₂*, 46th International Symposium of the American Vacuum Society, Seattle, WA, 1999.
- (58) Bode, M.; Pascal, R.; Wiesendanger, R. *Surf. Sci.* **1995**, *344*, 185.
- (59) Lüth, H. *Surfaces and Interfaces of Solids*; Springer-Verlag: Berlin, 1993.
- (60) Overbury, S. H.; Bertrand, P. A.; Somorjai, G. A. *Chem. Rev.* **1975**, *75*, 547.
- (61) Somorjai, G. A. *Chemistry in Two Dimensions: Surfaces*; Cornell University Press: Ithaca, NY, 1981.
- (62) Honig, R. E.; Kramer, D. A. *RCA Rev.* **1969**, *30*, 285. The vapor pressure of solid Cu at 300 K is not available here nor in ref 36. We have correlated the logarithm of vapor pressures for Cu at $T > 800$ K with the inverse of temperature (according to the Clausius–Clapeyron equation) to calculate the vapor pressure of Cu at 300 K, p_0 . The values of p_0 from both data sources (here and ref 36) agree.
- (63) Rodriguez, J. A.; Dvorak, J.; Jirsak, T. *Surf. Sci.* **2000**, *457*, L413.